Lab on a Chip

ARTICLE

Smartphone-App based point-of-care testing for myocardial infarction biomarker cTnI using an autonomous capillary microfluidic chip with self-aligned on-chip focusing (SOF) lenses

Received 00th January 20xx,
Accepted 00th January 20xx

DOI: 10.1039/x0xx00000x

www.rsc.org/

Chao Liang[a] , Yuanchang Liu[c], Aiying Niu[a], Chong Liu [a, b*], Jingmin Li[a*], Dianxiu Ning[d]

Cardiovascular disease is one of the most common causes of mortality in the world. Most of the diagnostic processes usually require bulky instruments and trained professionals, which cannot meet the demand for fast, early and regular bedside diagnosis. In this paper, a bespoke app on a smartphone and an autonomous capillary microfluidic chip (ACMC) are combined to realize the point-of-care testing of cardiac Troponin I (cTnI). The smartphone-app-ACMC platform was based on the sandwich immunofluorescence principle and featured the self-aligned on-chip focusing (SOF) lenses which can avoid the complex optical coupling process. The operator only needs to introduce 100µl sample into the ACMC, where the priming, time-delaying, mixing and washing steps for the assay can be accomplished automatically. With the help of the bespoke app and a palm-sized optical attachment, the smartphone can capture the fluorescence image, process the fluorescence intensity information, output the detection result and save the result for long-term monitoring. Our results showed that within 12min, the detection limit of 78 pg/ml and 94pg/ml for cTnI were attained in buffer and spiked human serum, respectively. Our proposed platform has the potential to be applied in the POCT field especially for some resource-limited settings.

Introduction

Cardiovascular disease is the leading cause of death globally[1] and consequently, places an ever-increasing burden on the healthcare service in both resource-rich and resource-limited settings. In cardiovascular diseases, myocardial infarction (MI) is one of the most immediately life-threatening forms[2]. According to the previous research, every 30 min delay of the diagnosis can increase the risk of 1-year mortality by 7.5%[3]. Meanwhile, up to 50% of patients exhibited normal or ambiguous readings of the electrocardiogram (ECG)[4], making the fast, efficient and accurate diagnosis become a crucial factor for saving the lives of the patients under the potential threats of MI. When it comes to the diagnosis of MI, presently, the cardiac biomarker troponin I (cTnI) is considered to be the gold standard biomarker, as only the direct damage of myocardium can result in the increasing concentration of cTnI [5-6]. Hence, the assessment of cTnI can assist with the clinicians in making decisions on a proper course of treatment in a more comprehensive manner.

With the benefits of being able to efficiently and effectively provide the diagnosis results, point-of-care testing (POCT) which can achieve on-site assay has attracted increasing interests in recent years [7-8]. POCT technology can provide the diagnosis results more efficiently and effectively. Using POCT, the diagnosis process can be conducted without bulky instruments and trained professionals, making such a technology an ideal option for fast, early and regular bedside detection of cTnI. The typical POCT device is based on the lateral flow technology, which has been used in the area such as the commercially available home pregnancy test strips. With the utilization of one or several layers of absorbent membranes, the lateral flow devices is able to direct the test sample to the biosensing area [9], and the test result can be obtained either from a visible color change on the test strips or some quantitative data from a separate analysis instrument [10]. However, for such devices, since the test sample is driven by the capillary force generated from the porous membranes, the different pore sizes of the membranes between batches can have a significant influence on the accurate control of fluidic flow, which could potentially cause an inaccurate result and also poor reproducibility. The microfluidic chip has advantages over the lateral flow device as they are fabricated using single and uniform materials, such as polymer [11], glass [12] and sillion [13], which can guarantee the accuracy of the flow rate. Various microfluidic networks can be established through microfabrication techniques, making it easy to integrate more functional elements. There were several POCT applications for detection of cTnI based on the microfluidic chips [14-16]. Although these applications were proven to be successful, most of the existing microfluidic platforms still involved multi-step sample introduction operations [14], which was unfriendly for the untrained patients. Also, extra power supply such as centrifugal instruments [15]

[a.] *Key Laboratory for Micro/Nano Technology and System of Liaoning Province, Dalian University of Technology, Dalian, China.*
[b.] *Key Laboratory for Precision and Non-traditional Machining Technology of Ministry of Education, Dalian University of Technology, Dalian, China.*
[c.] *Department of Mechanical Engineering, University College London, London, UK.*
[d.] *The First Affiliated Hospital of Dalian Medical University, Dalian, China*
† *E-mail: jingminl@dlut.edu.cn; chongl@dlut.edu.cn.*
‡ *Electronic supplementary information (ESI) available.*

or external pumps [16] was still required to propel the reagent, which was not ideal for POCT despite the use of miniaturized microchips. In addition, the development of true POCT was also severely hindered by the requirement of large, expensive and complex bench top imaging microscope for the quantitate analysis of the detection results [17-18].

Using a smartphone as the detection platform for POCT device has received a lot of research attention these days [19]. Compared with the microscope system, the smartphone is a highly-integrated intelligent device and has several advantageous features. For example, the smartphone has an integrated COMS component and a central processing unit (CPU), and it can capture the testing images with high resolution, process the image information and output the processing results on the same device. Also, when using the device, the operator only needs to touch a few buttons on the screen to complete the detection process under a friendly human-smartphone interaction. More importantly, as an almost indispensable communication tool, the patients can perform the test at home and directly send the detection results to the clinician's smartphone for the professional comments. While the smartphone-based device has made great contributions to the POCT field with many smartphone-based POCT applications been reported [20-25], there are still some key issues to be addressed. The multi-function features of the smartphone have not been fully exploited. In some applications, the smartphone was only utilized as an image capturing tool and the captured images have to be sent to the bench top computers for post-processing [20-21]. Besides, due to the limited capability of the smartphone CMOS, it is difficult to achieve a satisfied sensitivity level using the smartphone-based device. In order to solve this problem, microlenses [22-23] and waveguides [24-25] have been integrated in the smartphone-based device to enhance the signal intensity and further improve the sensitivity and detection limit of the device. However, most of the aforementioned formats required the use of large ancillary equipment, such as laser excitation sources, light guiding fibers and light collimators. The optical coupling process must be carefully conducted otherwise the detection performance will be obviously compromised. In the previous research, a planar microlens made of PDMS material was demonstrated to be able to amplify the fluorescence signal from a sample of fluorescent particles [26]. The microlenses were fabricated together with the microchannel making it can be self-aligned, and has the benefits of being capable of avoiding the complex light coupling process and ancillary equipment. However, in that work, a CCD or spectrometer was used as the detector and the results were processed through bench top computer, which negated many of the benefits from device miniaturization. In addition, no biological or chemical based assays have been carried out to verify the performance of the microfluidic system.

In this work, a smartphone-app-ACMC platform for point-of-care testing of myocardial infarction biomarker cTnI has been presented. For the assay, the sandwich immunofluorescence principle was based upon and the FITC-labelled antibody as well as the capture antibody was pre-immobilized on the surface of the ACMC. By only introducing 100μl sample into the ACMC by the operator, the priming, time-delaying, mixing and washing steps for the assay can be accomplished automatically. With the help of an android-based app and an optical attachment, the smartphone can then capture the fluorescence image, process the fluorescence intensity information, output the detection result and save the result for long-term monitoring. It should be noted that one of the important features that the proposed the platform possesses are the self-alignment on-chip focusing (SOF) lenses. These lenses were fabricated from PMMA material using CO_2 laser ablation process with the light emitting diode (LED) being used as the excitation source. As the core component of the platform, the geometry, material and types of the focusing SOF lenses have been analyzed theoretically and experimentally. Our results show that with the optimized lenses, 0.1pg/ml fluorescein isothiocyanate (FITC) solution can be successfully detected. Within 12min, the detection limit of 78pg/ml and 95pg/ml for cTnI have been obtained in buffer and spiked human serum with their R^2 of 0.983 and 0.972, respectively. Given that the clinically applicable concentration was 0.01–0.1 ng/ml [27-28], the proposed platform has the potential to be used in the clinical applications.

Experimental section

Configuration of the smartphone-app-ACMC platform

Fig. 1a shows the schematic diagram of the smartphone-app-ACMC platform. It can be seen that the platform comprises three parts,

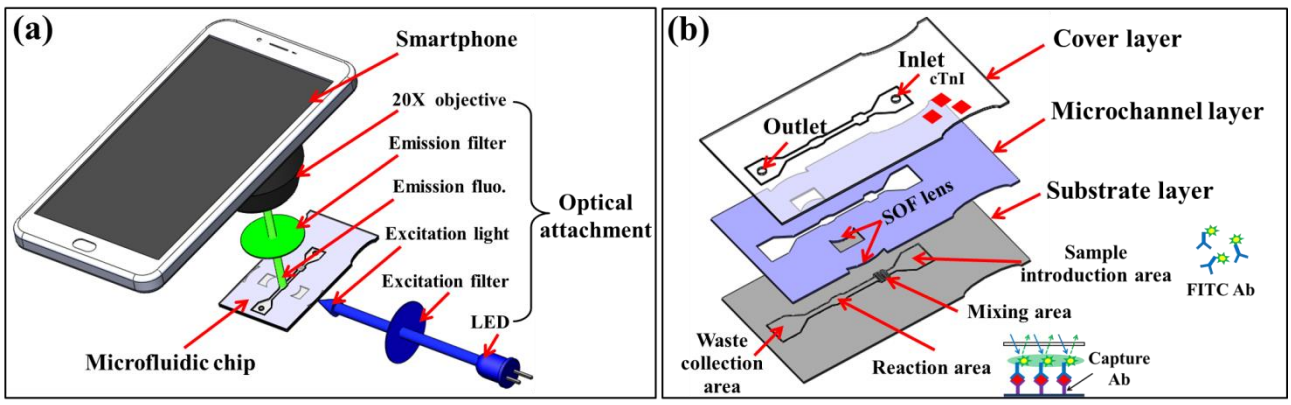

Fig.1 (a) Schematic diagram of the smartphone-app-ACMC platform. (Fluo. indicates fluorescence.) (b) Schematic diagram of the ACMC. .

which are smartphone, optical attachment and ACMC. The smartphone model used in this work was Meizu MX 5, which has a 20.7Mpixel color RGB sensor with F/2.0 aperture and 28 mm focal length lens. Within the optical attachment, two blue LED excitation sources (Telesky, China), two band pass excitation filters with the center wavelength of 490±3nm (Feiyuda, China), one band pass emission filter with the center wavelength of 530±3nm (Feiyuda, China) and one 20x microscope objective (SAGA, China) were housed within the optical attachment. The LED excitation sources and excitation filters were placed at the distance of about 3mm from each side of the ACMC, respectively, making the excitation light orthogonal to the fluorescence emission (The Fig. 1a only demonstrates one side for simplicity). The optical attachment was fabricated from black PMMA sheets using CO_2 ablation process and assembled using bolts.

The ACMC consists of three layers, including the cover layer, the microchannel layer and the substrate layer (Fig. 1b). On the cover layer, there are an inlet to introduce the testing sample and an outlet to vent the air in the microchannel. The SOF lens and the microchannel side walls are integrated on the microchannel layer. The substrate layer is applied to form a sealed chamber of the ACMC. There are four functional areas integrated on the ACMC, which are the sample introduction area, the mixing area, the reaction area and the waste collection area. As the 100 μm cTnI spiked sample is introduced into the sample introduction area, the FITC labelled antibody (FITC Ab), which is pre-immobilized in this area, can be washed off and flow into the mixing area. In the mixing area, the testing sample and the FITC Ab are fully mixed due to the saw tooth structure generated by the CO_2 laser ablation. The saw tooth structure can disrupt the flow and thus induce a chaotic mixing performance [29].

Fabrication of the ACMC

Each layer of the ACMC is fabricated from PMMA sheets (Asahi, Kasei) using CO_2 laser ablation process. The commercially available CO_2 ablation system with a 50w laser generator (JinBoshi JBSCO$_2$-50) was used in the experiments. The length and width of the ACMC are 60mm and 30mm, respectively. The thickness for the cover layer, microchannel layer and substrate layer is 1mm, 0.5mm and 1mm, respectively. For the microchannel layer, the pattern of the microchannel and the microlens was scanned through the 0.5mm thick PMMA sheet, producing microfluidic channel and the SOF lens of a height dictated by this thickness. Subsequent to the CO_2 laser ablation process, microchannel side walls and the SOF lens surface were sequentially sanded with 800, 1000 and 2000 grit sandpapers and finally polished with a specialized polymer polishing paste (SONAX30500, Germany). Subsequent to the laser-ablation process, the three layers were bonded using the laser-bulge ultrasonic bonding method. This bonding method has been systematically studied in our previous research [30-31] and therefore the proposed method will not be described in detail here. The detailed fabrication process and processing parameters can be found in the supplementary information S1.

Development of the Android-based app

In order to make full use of the imaging capturing and data processing capability of a smartphone, a bespoke app has been developed. The app was programmed using an android developer software Eclipse and tested on a Meizu MX5 smartphone running android 8.1.0. Using such an app, by touching a few buttons on the screen by the operator, the smartphone can perform a series of operations of capturing the fluorescence image, extracting the fluorescence intensity from the image, outputting the detection results and saving the results for long-term monitoring. The operation procedure of the app can be described as follows:

1) When the operator touches the app icon, the main menu will display on the screen (Fig. 2a) with four options in this interface being displaced as: New Test, History, Instruction and Quit.

2) When the "New Test" option is selected, the app turns to the image capture interface (Fig. 2b), within which, a white box with a resolution of 240×360 pixels identifies the capture area. When the operator click on the "Capture" option, the image within the white box will be taken and directly saved in the smartphone's internal memory for further analysis.

3) Subsequently, the operator clicks on the "Ansys" option and the detection results including RGB (red, green and blue) value, fluorescence intensity and concentration will be displayed on the screen (Fig. 2c).

4) Finally, the operator can select the "Save" option to save all the detection result in the smartphone as well as the detection date and serial number (Fig. 2d).

The fluorescence images saved in the smartphone are in a RGB color space and its intensity can be obtained by converting the RGB values into the luminosity value according to the following expression [32]:

$$I = 0.30R + 0.59G + 0.11B \quad (1)$$

where I indicates the fluorescence and R, G, B mean the red, green and blue pixel intensities in their respective color channels. The detailed image processing method and code are demonstrated in the supplementary information S2. The concentration value demonstrated in the detection results interface was determined by the calibration equation. The calibration equation and the correlation coefficient were calculated using the least square method based on the concentrations of cTnI spiked standard solutions.

Detection of FITC solution

Before the immunofluorescence assay for cTnI, the detections of FITC solutions with various concentrations were carried out to validate the performance of the different types of SOF lenses. The FITC dye was first made into a stock solution with ethanol according to the manufacture's specification, and then diluted into the desired concentration with deionized water. The FITC solutions with the concentrations of 0.01mg/ml, 1μg/ml, 0.1μg/ml, 0.01μg/ml, 1ng/ml, 0.1ng/ml, 0.01ng/ml, 1pg/ml, 0.1pg/ml and 0.01pg/ml were prepared. In addition, the DI water without the FITC was used to be a blank control group. These FITC solutions and DI water were then introduced into the ACMC with no SOF lens, single SOF lens and compound SOF lens, respectively. With the help of the aforementioned app, the corresponding fluorescence intensities were obtained from the smartphone. Each detection was conducted three times with separate ACMCs. In order to achieve a quantitative analysis for each fluorescence image, the fluorescence

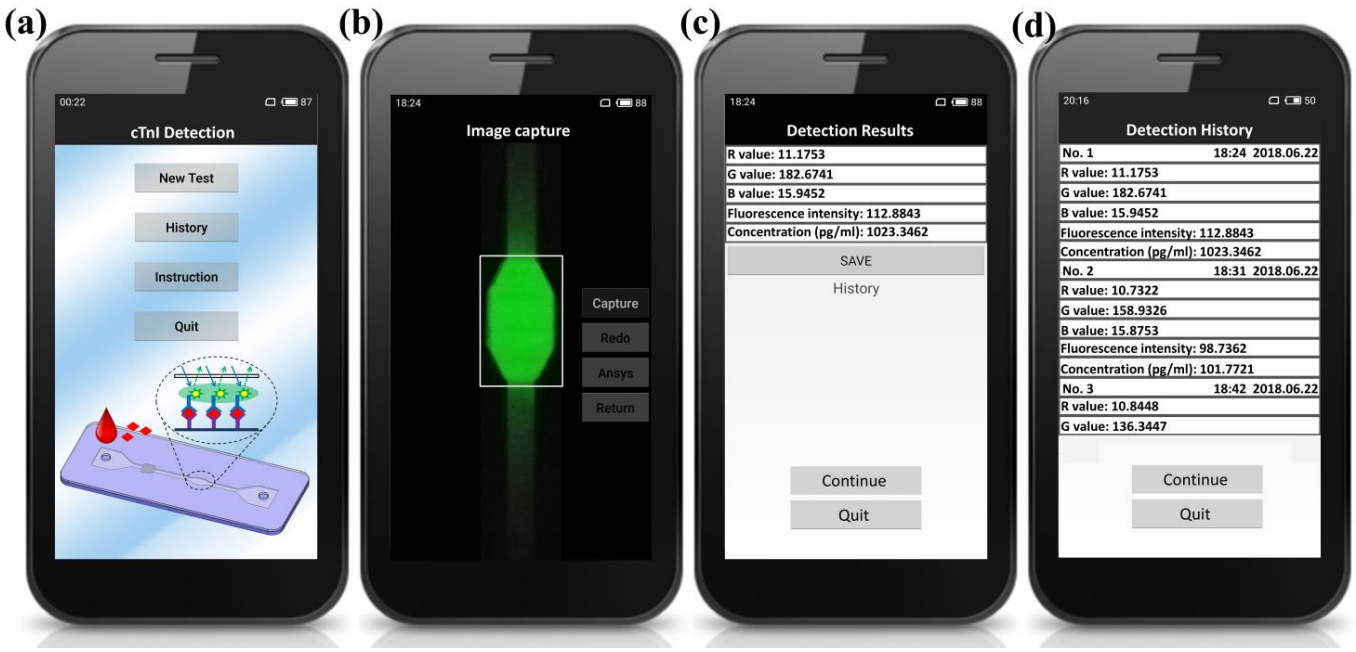

Fig.2 Screenshot images for each functional interface. (a) Main menu interface. (b) Image capture interface. (c) Detection results interface. (d) Detection history interface.

images were also processed by Matlab and the detailed processing code is presented in the supplementary information S3.

Immunofluorescence assay for cTnI

A sandwich style immunoassay configuration was used to carry out the fluoroimmunoassay, where the FITC Ab and capture Ab were immobilizedon the surface of the substrate layer of the ACMC. Before the antibody immobilization process, the substrate was submitted to UV/ozone treatment using the controllable gradient UV irradiation (CGUI) method reported in our previous research [33]. This method can render the surface of the substrate layer selective wettability, which, as a result, can tune the flow rate in the microchannel and achieve different immobilization performance on the surface.

In this work, the method demonstrated in our previous work[33] was performed as follows. Four pieces of quartz plates (Jinghe, China) were sputtered with different thickness of Cu and subsequently arranged on top of the four functional areas. The Cu film was used to control the UV irradiation which was transmitted to the functional area surface and the corresponding modification performance can thus be varied based on our expectation. For the sample introduction area and reaction area, no quartz plates were arranged on their surfaces, making both the areas treated with complete UV irritation. The quartz plate with the Cu sputtering time t of 11s and UV transmittance T of about 10% was arranged on the mixing area and the quartz plate with t of 5s and T of about 40% was arranged on the reaction area.

Subsequent to the UV/ozone treatment using the CGUI method, the next step is to perform the antibody immobilization process. FITC labeled human specific monoclonal anti-cardiac cTnI detection antibodies, human specific monoclonal anti-cardiac cTnI capture antibodies, and human cTnI biomarkers used in this work were all provided by Wondfo Ltd. (Guangzhou, China). FITC Ab and capture Ab were diluted into 0.4mg/ml and 60μg/ml respectively with phosphate buffered saline (PBS, pH 7.4). 1.5μl capture Ab. solution was spotted onto the reaction area of the substrate layer using a non-contact spotter developed by our group and incubated at 30 °C for 2 hours subsequent to the spotting process. Then, the substrate layer was washed three times with PBS buffer to remove any unbound antibodies. After the substrate layer was dried, the layer was immersed in a 1mg/ml solution of bovine serum albumin (BSA) and incubated for 30min at room temperature, which was meant to minimizing the non-specific binding of the reaction antigen. Next, the substrate layer was washed three times with PBS buffer to remove any unbound/residual BSA. Finally, 3μl FITC Ab. was spotted on the sample introduction area of the substrate layer and incubated at 30 °C for 1 hour. Then, the three layers of the ACMC were sealed using the laser-bulge based ultrasonic bonding method. It should be noted that while the immobilization performance on the PMMA surface can be improved through some chemical modification method[34], such technology involves multi-step treatment procedures. Consider that antibodies can be immobilized passively onto the PMMA surface by direct incubation[35], the passive immobilization method was adopted in this work. The cTnI biomarker samples with the concentration of 100ng/ml, 50ng/ml, 15ng/ml, 8ng/ml, 3ng/ml, 0.5ng/ml and 0.1ng/ml were prepared in PBS buffer as well as in human serum (YareWell, China) for analysis. The minimum concentration of 0.1ng/ml was selected because it is within the range of clinically acceptable concentrations of cTnI biomarker (0. 01–0.1 ng/ml) [27-28] before the occurrence of an acute myocardial infarction.

Results and discussions

Geometry analysis and material selection for the SOF lens

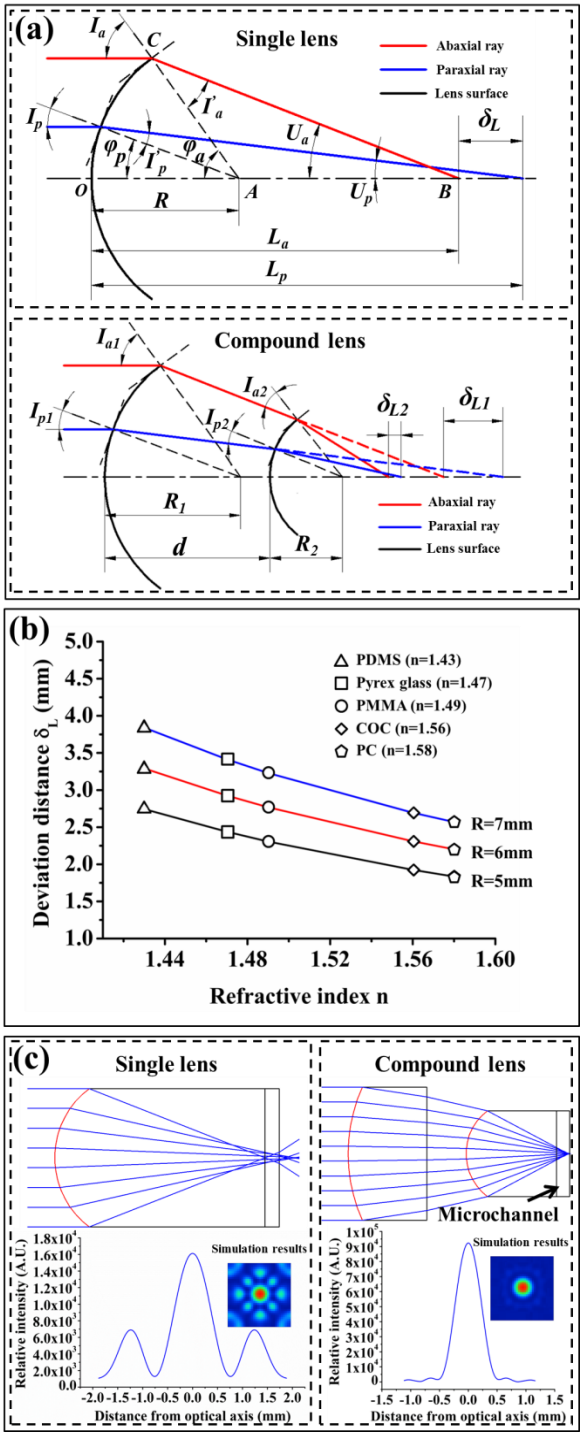

Fig.3 (a) Geometry analysis of the single and compound SOF lens. (b) The relationship between the refractive index and the deviation distance. (c) Optical simulation results for SOF lenses (comparison between the single lens and the compound lenses)

The SOF lenses are fabricated together with the microchannel on the same layer, making the optical axis of the planar SOF lenses being able to be self-aligned to the vertical plane of the reaction area. The SOF lenses and the reaction area can be directly coupled to the LED excitation source without any ancillary equipment. However, the geometry of the SOF lenses cannot be changed after the fabrication process making them have to be optimized to match the whole optical system.

Firstly, the influence of the lens geometry on the focusing performance is analysed. The lens with the convex features has the focusing capability. However, due to the curvature of the lens, the abaxial ray and paraxial ray cannot focus on the same point, which can result in the decreasing of light intensity in the focusing area. Here, the abaxial ray means the ray at the rim of the lens, which is far away from the lens center and the paraxial ray is near the center of the lens as shown in Fig. 3(a). The deviation distance δ_L of the focus point between the abaxial ray and the paraxial (deviation distance for short) can be expressed as follows:

$$\delta_L = \frac{R}{n}\left\{\frac{\sin I_p}{\sin\left[I_p - \arcsin\left(\frac{\sin I_p}{n}\right)\right]} - \frac{\sin I_a}{\sin\left[I_a - \arcsin\left(\frac{\sin I_a}{n}\right)\right]}\right\} \quad (2)$$

where R is the curvature radius of the lens and n is the refractive index of the material. I_a and I_p denote the incident angle of the abaxial ray and paraxial ray, respectively. The detailed derivation process of Eq. (2) can be found in supplementary information S4. Based on Eq. (2), the deviation distance δ_L as a function of the refractive index was calculated analytically as given in Fig. 3(b), where I_a and I_p were given 50° and 5°, respectively.

The results in Fig.3(b) reveals that as the refractive index increases, the deviation distance δ_L reduces. As seen in Fig.3(b), with the lens radius of 6mm, the deviation distance δ_L for PDMS (n=1.43), Pyrex glass (n=1.47), PMMA (n=1.49), COC (n=1.56) and PC (n=1.58) is 3.29mm, 2.92mm, 2.76mm, 2.31mm and 2.21mm, respectively. It can be seen that although the deviation distance δ_L is decreased with the increasing of refractive index, the increasing trend is not obvious. For PMMA and PC, the deviation distance δ_L only decreases about 0.5mm. Moreover, the compatibility of PMMA material and laser-ablation process is better than other materials. For PDMS, the laser cannot ablate the material surface and for PC, the laser can completely burn the material surface. Additionally, the antibody can be passively immobilized on the PMMA surface[35], which is crucial for the following immunofluorescence assay. Therefore, the PMMA material is selected in our work.

In order to decrease the deviation distance δ_L, another lens is added to complete a compound lens format. Through the second lens, the light can be further focused, which can obviously decrease the deviation distance. The expression of the deviation distance δ_{L2} for the compound lens was derived (See S4 for detail). Based on the expression, it can be calculated that when another lens with the radius of 3mm is added to the first lens with their distance of 7mm, the deviation distance δ_{L2} can be decreased to 0.67mm. To be compared, the deviation distance δ_{L1} of the single lens is 2.76mm.

Table 1 Dimension of the SOF lenses. (Unit: mm)

	First lens				Second lens		
	First surface radius	Second surface radius	Lens thickness	Distance to the next surface	First surface radius	Second surface radius	Lens thickness
Single lens	6	∞	16.5	_	_	_	_
Compound lenses	12	∞	6	3	4	∞	7.5

In both situations, the radius of the first lens and the incident angle of the abaxial ray and paraxial ray remain the same, which are 6mm, 50° and 5°.

By using the software Zemax 2009, the radius and the distance between the two lenses of the compound lens can be optimized. The focus point was set to the center of the reaction area of the ACMC. And considering the dimension of the ACMC, the focus length was given as 16.5mm. The optimized result of the lenses was listed in Table 1. After the optimization, the deviation distance δ_{L2} was reduced to 0.32mm. Fig.3(c) shows the optimization result. From Fig.3(c), it can be seen for the single SOF lens, a large deviation distance was formed which clearly reduced the intensity of the focusing light compared with that of the compound SOF lens where the deviation distance δ_{L1} was minimized. It should be noted that in order to have a simplified fabrication process, only the compound SOF lens comprised of two single SOF lenses has been investigated in this study.

Characterization of the smart-app-ACMC platform

The smartphone with the bespoke app was attached to the palm-sized optical attachment (105mm in length, 85mm in width and 40mm in height) through a phone clip (Fig. 4a). A battery compartment was mounted on the side of the optical attachment with two AAA batteries (each battery of 1.5V), which provided the power for the LED light source. The operation procedure has been designed in an easy way that the user first introduces the test sample into the ACMC (Fig.4b i)) and waits for about 12 min to let the immunofluorescence assay completed. Then, the ACMC is inserted into the chip slot, which is located at the rear of the optical attachment. Finally, after turning on the power switch, users can run the app in the smartphone according to the operation instruction with the detection results been displayed in seconds.

The pattern of the SOF lens and microchannel was directly scanned to the ACMC using the CO_2 laser ablation process. Compared with other microfabrication processes, which usually require the photolithography and etching technologies, the CO_2 laser ablation process is fast and cost-effective. However, due to the nature of the ablation process and the limitations of the stepper motor used to move the laser beam, defects generated on the surface of the microlenses were also inevitable. In Fig.4b ii), some hillocks and pits structures can be observed on the surface of the microlenses without the polishing process and the average surface roughness Ra was as high as 5.326μm measured by a white-light interferometer (New view5022, ZYGO, USA). These defects had a significant influence on the transparency of the PMMA material, which was detrimental to the focusing performance. However, such defects can be almost entirely removed using the polishing process of the PMMA surface. It can be seen from Fig.4b ii), subsequent to the sanding process with the various sandpapers and the polishing processing with the polymer polish paste, the average surface roughness Ra was decreased to 0.302μm.

The bonding accuracy is crucial for the microfluidic chips, especially for the capillary-driven ones. Based on the capillary flow analysis, the flow rate is determined by the viscosity of the liquid, the wettability and geometry of the microchannel[36] and the bonding quality can significantly affect the geometry of the microchannel in the height direction, which can cause the unexpected variation of the flow rate in the microchannel. In this work, the laser-bulge based ultrasonic bonding method was applied to achieve an accurate bonding performance. As the ultrasonic energy is exerted to the bonding chips, the heat generated from the ultrasonic energy is concentrated on the laser bulge (LB) and thus the microchannel is still rigid enough to endure the bonding pressure and will not deform after the bonding process. When the LB is melted, it will flow into the laser-formed groove, preventing the LB flowing into the microchannel or leaving a small gap between the bonding interfaces. Due to the aforementioned features, the dimension variation before and after bonding was not detectable as shown in Fig.4b iii).

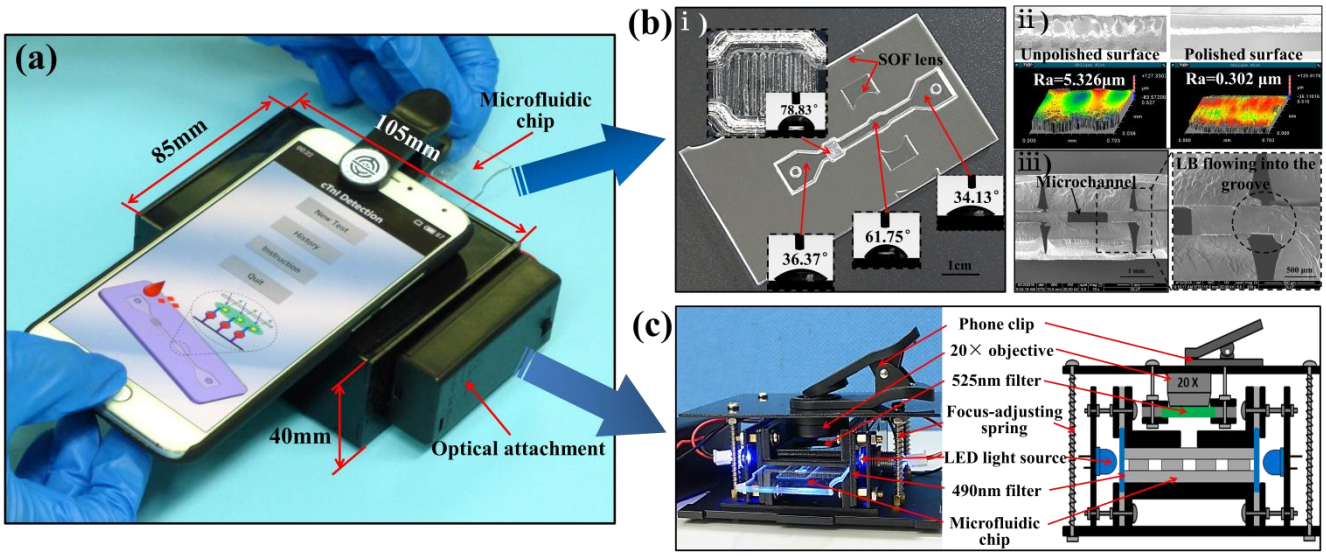

Fig.4 Characterization of the smart-app-ACMC platform. (a) Pictures of the complete smartphone-app-ACMC platform. (b) Charaterization of the ACMC. i) The picture of the ACMC. ii) Comparison between the unpolished and polished surface of the SOF lens. iii) Cross-section image of the bonded ACMC. (c) The components and their relative positions inside the optical attachment.

Fig. 4c shows the components and their relative positions inside the optical attachment. It can be seen that two blue LEDs was used as the excitation source as an alternative to the laser source. This is because LEDs are cost effective, able to produce high luminosities, have relatively low power consumption and can be easily to be integrated into miniaturized platforms. However, the LED sources are broadband and have large half angles of emission. Therefore, in the proposed platform, the SOF lenses were applied to focus the dispersed light and the 490nm band-pass optical filters were used to narrow the band of the excitation source. It can also be seen that the LED sources were placed on the side of the ACMC, making the excitation light orthogonal to the fluorescence emission light. By using the orthogonal optical path, the noise from LED can be largely avoided, which can potentially improve the detection sensitivity of the system. According to the inverse-square law, the light intensity is inversely proportional to the square of the distance from the light source, which means if the smartphone camera is placed at a long distance from the ACMC, the intensity of the fluorescence emission signal detected by the camera CMOS will be severely decreased. However, due to the limited macro shooting capability of the smartphone camera, if the focusing distance is less than 8cm, the clear image cannot be obtained. In order to address this issue, a 20x objective was added in the optical attachment and coupled to the smartphone camera with a phone clip. It should be noted that the focus adjustment mechanism is used to adapt to the different smartphone models, since different smartphone may have different focusing performances. That is to say the focus adjustment process needs to be conducted only once for the same smartphone device. With the 20x objective, the focusing distance can be decreased to about 2mm, which significantly improve the detection performance of the camera COMS.

Validation of the SOF lens through FITC detection

In order to validate the focusing ability of the different types of SOF lens, the FITC fluorescence detection experiments were performed with 0.01mg/ml, 1μg/ml, 0.1μg/ml, 0.01μg/ml, 1ng/ml, 0.1ng/ml, 0.01ng/ml, 1pg/ml, 0.1pg/ml and 0.01pg/ml concentrations of FITC fluorescence solutions using the proposed smartphone-app-ACMC platform. Fig. 5a, fig. 5b, and fig. 5c show the fluorescence images and the intensity profiles using no SOF lens, single SOF lens and compound SOF lens, respectively. The concentration of the FITC fluorescence solution was 1μg/ml. It can be seen that with the compound SOF lens, the excitation light focused on the reaction area, which was coincident with the design results, making the fluorescence emission intensity almost four times higher than that without the SOF lens. The derivation distance of the single SOF lens is larger than that of the compound SOF lens. The derivation distance resulted in the dispersed fluorescent beam profile, which caused the fluorescence intensity about 40% lower than that with the compound SOF lens. Fig. 5d shows the comparison of the fluorescence intensity between different types of SOF lens with the various concentrations of the FITC solutions. It can be seen that without the SOF lens, as the concentration of the FITC solution was less than 0.01ng/ml, the fluorescence intensity was almost the same with that of blank control sample (DI water), which indicated that the detection limit of the platform was about 0.01ng/ml. In comparison, with the compound microlens, when the FITC solution concentration was 0.1pg/ml, the fluorescence intensity was still clearly above the intensity of the blank control sample. An inverted fluorescence microscope (Olympus IX71) is applied to evaluate the fluorescence intensity of the FITC solution. The testing result showed that the detection limit of the FITC using the microscope is

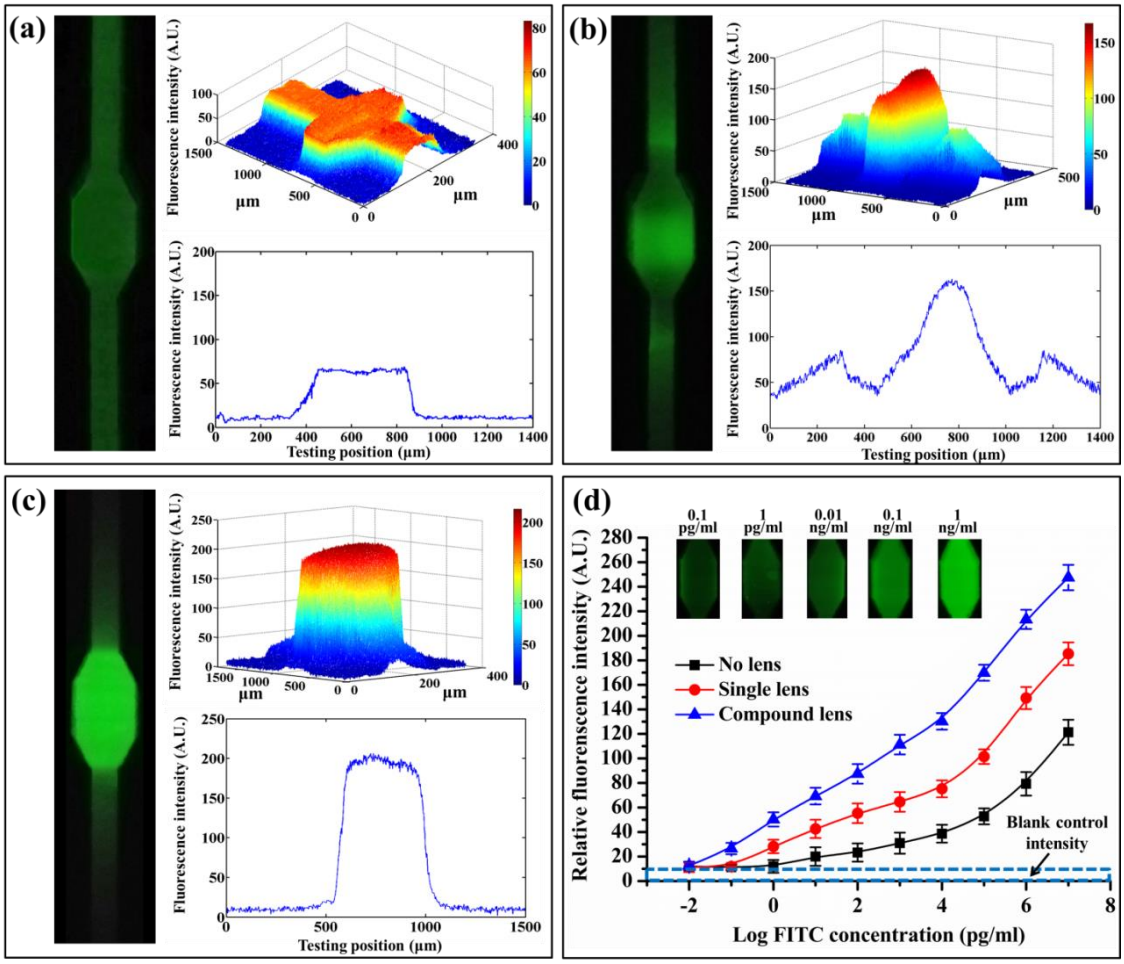

Fig.5 Validation of the SOF lenses. (a) Fluorescence image and the intensity profile with no SOF lenses. (b) Fluorescence image and the intensity profile with single SOF lenses. (c) Fluorescence image and the intensity profile with compound SOF lenses. (d) Comparison of the fluorescence intensity between different types of SOF lenses with various concentrations of the FITC solutions. Insert: representative fluorescence images using the compound SOF lenses.

about 0.03pg/ml, which is lower than that of our proposed platform. However, considering the portability and friendly operation capability, our platform still has advantages especially in the POCT field.

cTnI immunofluorescence assay

Fig.6 shows the results for the cTnI immunofluorescence assay. During the assay process, the flow rate of the sample solution is vital for the testing results. For example, in the sample introduction area, a fast flow rate is required to wash off the FITC Ab, and in the mixing area, a low flow rate is preferred to make the cTnI antigen fully mix with the FITC Ab and bind to it. Similarly, in the reaction area, the flow rate should be relative slow to let the remaining free epitope of the targeted antigen bind to the capture Ab. Finally, in the waste collection area, a fast flow rate can rapidly remove the unbound reagents and decrease the background fluorescence. The flow rate can be turned by the selective wettability of the four functional areas. From Fig.4b i), it can be seen that subsequent to 7min UV/ozone treatment using the CGUI method, the selective wettability was rendered to the four functional areas. The water contact angles (WCAs) for the sample introduction area, the mixing area, the reaction area and the waste collection area were 36.37°, 78.83°, 61.75° and 34.13°, respectively. The flow rate in a capillary-driven microchannel is determined by the viscosity of the liquid, the wettability and geometry of the microchannel. Therefore, by varying the wettability of the microchannel, the cTnI spiked solution took about 30s, 4min, 6min and 50s to fill the sample introduction area, the mixing area, the reaction area and the waste collection area, respectively. The whole assay time took about 12 min. It can be found that the FITC Ab can be washed off from the sample introduction area while the capture Ab. remains on the reaction area which is a key feature to achieve the one-step assay. The reason for such a phenomenon can be attributed to the following two factors. Firstly, it has been reported that the surface wettability plays an important role in protein adsorption and in most cases more hydrophilic surfaces inhibits the absorption of proteins [37-38]. In our cases, it can be seen that the WCA of the sample introduction area where the FITC Ab. was immobilized was about 20° lower than that of the reaction area where the capture Ab was immobilized and thus, the more hydrophilic surface decreased the

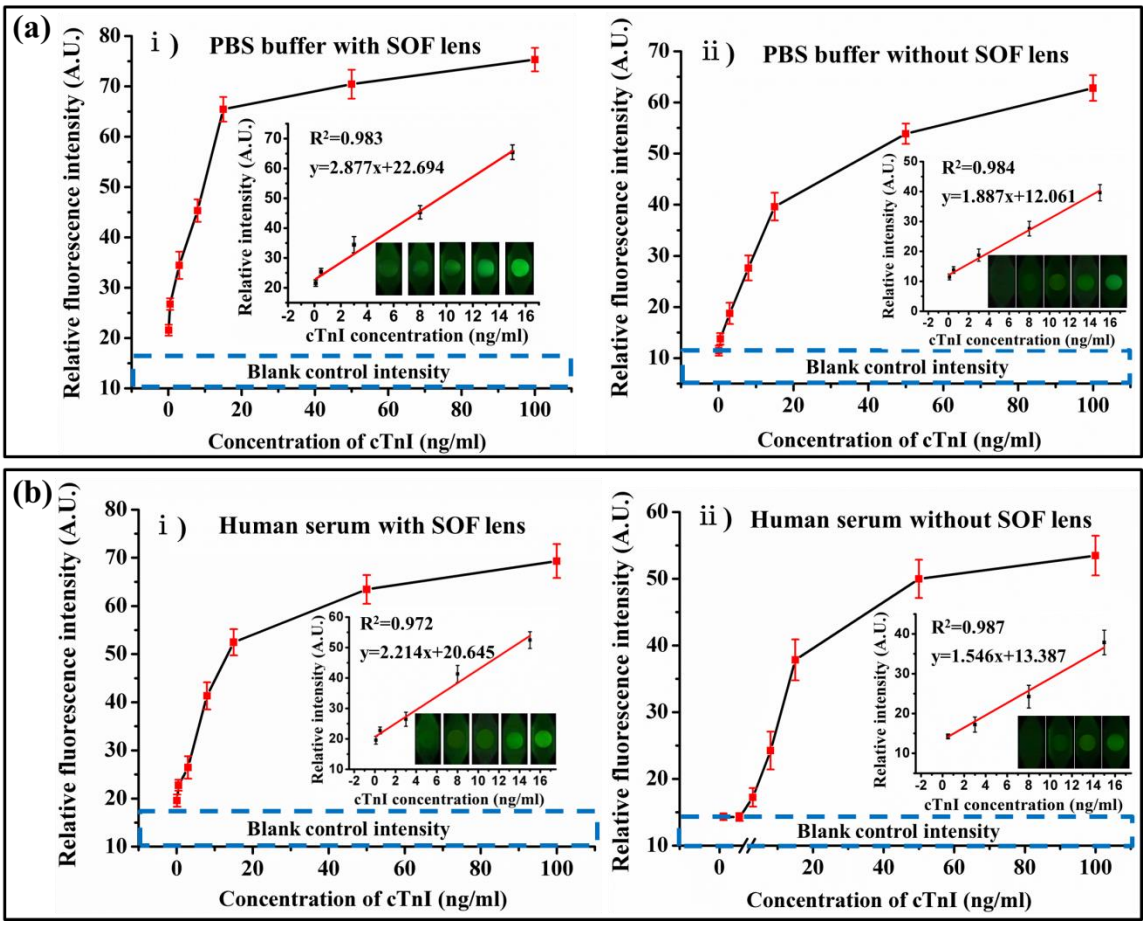

Fig.6 The curves of the relative fluorescence intensity versus the cTnI concentration in (a) PBS buffer and in (b) human serum with and without the SOF lens. Insert: the linear calibration curve between the relative fluorescence intensity and the cTnI concentration in the range of 0.1ng/ml to 15ng/ml.

immobilization strength of the FITC Ab. The second factor is that based on the capillary flow theory, the decreasing geometry and more hydrophilic property of the sample introduction area can provide stronger capillary pressure to wash off the FITC Ab.

The relationship between the fluorescence intensity and the cTnI concentration in PBS buffer was established, which can be seen from the curve in fig. 6a. It can be seen from fig. 6a i) that by using the SOF lens, the fluorescence intensity from the lowest cTnI concentration of 0.1ng/ml was still higher than that of the blank sample. A calibration curve (y=2.877x+22.694) was obtained with R^2=0.983 in the range from 0.1ng/ml to 15ng/ml. The lower detection limit (LDL) was calculated from the sum of the mean signal and 3 fold standard deviation (SD) obtained from the 20 fold blank sample measurements. The LDL was found to be approximately 78 pg/ml. In contrast, without the SOF lens, when the cTnI concentration was as low as 0.1ng/ml, the fluorescence intensity was almost the same as that of the blank sample. In this situation, the calibration curve was y=1.887x+12.061 with R^2=0.984 and the LDL was about 390pg/ml.

To evaluate the performance of the smartphone-app-ACMC device for real samples, human serum spiked with cTnI was tested. The result in fig. 6b shows that by applying the SOF lens, the calibration curve was linear over the range of 0.1 ng/ml–15 ng/ml and the LDL was 94pg/ml for cTnI in human serum (fig. 6b i), right inset, y = 2.214x + 20.645, R^2 = 0.972). Fig. 6b ii) shows the cTnI detection results in human serum without the SOF lens. The results in fig. 6b ii) reveal that the fluorescence intensity of the cTnI with the concentration lower than 0.5ng/ml cannot be distinguished from the blank sample and the LDL was about 550pg/ml (y = 1.546x + 13.387, R^2 = 0.987 in the range of 0.5ng/ml-15ng/ml). It can be noted that the LDL of cTnI in human serum was higher than that in PBS buffer. That is probably because the human serum adsorbed on the capture antibody non-specifically and decreased the capture site for the cTnI antigen.

The LDL of 78pg/ml and 94pg/ml for cTnI in PBS buffer and human serum was not the lowest compared to the results in other researches. The LDL, which was as low as 6.7pg/ml [39] and 10pg/ml [40], for cTnI was previously reported. However, they all involved multi-step assay processes, external fluid-driving and bulky result-analysing equipment. Besides that, the LDL of 94pg/ml is still within the range of clinically acceptable cTnI detection concentrations (0.01–0.1 ng/ml), demonstrating its potential application in the POCT field.

Conclusions

In this paper, a smartphone-app-ACMC platform has been proposed and demonstrated for point-of-care testing of myocardial infarction biomarker cTnI. The platform featured a bespoke app and an ACMC integrated with the SOF lens. By applying the proposed ACMC, the steps of priming, time-delaying, mixing and washing for the immunofluorescence assay can proceed automatically. With the help of the bespoke app, the smartphone can capture the fluorescence image, analyse the fluorescence intensity information, output the detection result and save the result for long-term monitoring, which facilitates the remote operation of the assay process, and is ideal for the requirement of POCT. The proposed SOF lens can self-aligned to the microchannel, by avoiding the complex optical coupling process. Compared with the platform without the SOF lenses, the FITC fluorescence intensity increased about four times for the platform with compound microlens, which achieved the detection limit of 0.1pg/ml for the FITC solution. In addition, the proposed platform displayed good specificity and sensitivity for cTnI antigen, with the LDL of 78 pg/ml and 94 pg/ml in PBS buffer and spiked human serum, respectively. It can be anticipated that the presented platform technology has the potential to be used as an applicable tool for diagnosing other clinical diseases or monitoring treatment efficacy in resource-limited settings.

Acknowledgements

This work was supported by the National Natural Science Foundation of China (51475079, 51375076), Science Fund for Creative Research Groups of NSFC (51621064) and Scientific research fund of Dalian science and technology bureau (2015E12SF164). This work was also supported by Fundamental Research Funds for the Central Universities (DUT15LAB12, DUT16TD20) and Natural Science Foundation of Liaoning Province (201602155).

References

1 A. Timmis, N. Townsend, C. Gale, R. Grobbee, N. Maniadakis, M. Flather, E. Wilkins, L. Wright, R. Vos, J. Bax, M. Blum, F. Pinto and P. Vardas, *Eur. Heart. J,* 2018,39,508–577.

2 M. I. Mohammed and M. P. Y. Desmulliez, *Lab Chip*, 2011,11,569-595.

3 G. D. Luca, H. Suryapranata, J. P. Ottervanger, and E. M. Antman, *Circulation,* 2004,109,1223-1225.

4 B. D. McCarthy, J. R. Beshansky, R. B. D'Agostino, H. P. Selker, *Ann. Emerg. Med,* 1993,22,579-582.

5 M. J. Holzmann, *J. Intern. Med,* 2018,284,50-60.

6 F. S. Apple, *Clin. Chem,* 2009,55,1303-1306.

7 C. D. Chin, V. Linder and S. K. Sia, *Lab Chip,* 2012,12,2118-2134.

8 L. Gervais, N. de Rooij and E. Delamarche, *Adv. Mater, 2011,23,* H151-H176.

9 J. Hu, Z. L. Zhang, C. Y. Wen, M. Tang, L. L. Wu, C. Liu, L. Zhu and D. W. Pang, *Anal. Chem,* 2016,88,6577-6584.

10 A. Warsinke, *Anal. Bioanal. Chem,*2009,393,1393-1405.

11 J. Wang, Z. Xu, H. Z, S. Hu, D. Wang, J. Liu and L. Wang, *Microfluid. Nanofluid,* 2017,21,27.

12 A. K. Bavil and J. Kim, Analyst, 2011,143,3335-3342.

13 M. Zimmermann, H. Schmid, P. Hunziker and E. Delamarche, *Lab Chip,* 2007,7,119-125.

14 P. Novo, F. Volpetti, V. Chu and J. P. Conde, *Lab Chip,* 2013,13,641-645.

15 W. Lee, J. Jung, Y. K. Hahn, S. K. Kim, Y. Lee, J. Lee, T. H. Lee, J. Y. Park, H. Seo, J. N. Lee, J. H. Oh, Y. S. Choi and S. S. Lee, *Analyst* , 2013,138,2558-2566.

16 B. Mosadegh, T. B. Begey, J. Y. Park, M. A. Burns and S. Takayama, *Lab Chip,* 2011,11,2813-2818.

17 L. Gervais, M. Hitzbleck and E. Delamarche, *Biosens. Bioelectron,* 2011,27,64-70.

18 L. Gervais and E. Delamarche, *Lab Chip,* 2009,9,3330-3337.

19 D. Zhang, Q. Liu, *Biosens. Bioelectron,* 2016,75,273-284.

20 F. Li, H. Li, Z. Wang, J. Wu, W. Wang, L. Zhou, Q. Xiao and Q. Pu, *Sens. Actuators B. Chem.* 2018,271,189-194.

21 H. Zhu, S. Mavandadi, A. F. Coskun, O. Yaglidere and A. Ozcan, *Anal. Chem.* 2011,83,6641–6647.

22 J. Hsieh, C. J. Weng, H. L. Yin, H. H. Lin and H. Y. Chou, *Microsyst.Technol,* 2005,11,429–437.

23 B. R. Watts, Z. Zhang, C. Q. Xu, X. Cao and M. Lin, *Electrophoresis*, 2014,35,271–281.

24 Q. Pu, O. Oyesanya, B. Thompson, S. Liu and J. C. Alvarez, *Langmuir,* 2007,23,1577-1583.

25 M. Fleger and A. Neyer, *Microelectron. Eng,* 2006,83,1291–1293.

26 J. Seo and L. P. Lee, *Sens. Actuators B. Chem ,* 2004,99,615–622.

27 B. McDonnell, S. Hearty, P. Leonarda and R. O'Kennedy, *Clin. Biochem,* 2009,42,549–561.

28 D. A. Morrow, C. P. Cannon, R. L. Jesse, L. K. Newby, J. Ravkilde, A. B. Storrow, A. H. B. Wu and R. H. Christenson, *Clin. Chem.* 2007,53,552–574.

29 A. D. Stroock, S. K. W. Dertinger, A. Ajdari, I. Mezić, H. A. Stone and G. M. Whitesides, *Science,* 2002,295,647-651.

30 C. Liang , C. Liu , Z. Liu , F. Meng and J. Li, *J. Micromech. Microeng,* 2017,27,115012.

31 C. Liang, F. Meng, J. Li and C. Liu, *Technol,* 2018,252,25–33.

32 A. Almuntashri and S. Agaian, IEEE international conference on systems man and cybernetics (SMC), 2010,10-13 Oct,3942-3947.

33 C. Liang, Y. Liu, C. Liu, X. Li, L. Chen, C. Duan and J. Li, *Sens. Actuators B. Chem,* 2018,273,1508–1518.

34 S. Wang, M. Esfahani, U. A. Gurkan, F. Inci, D. R. Kuritzkes and U. Demirci, *Lab Chip,* 2012,12,1508–1515.

35 M. I. Mohammed and M. P. Desmulliez, *Biomicrofluidic,* 2013,7,064112.

36 A. Fatona, Y. Chen, M. Reid, M. A. Brook and J. M. Moran-Mirabal, *Lab Chip,* 2015,15,4322–4330.

37 J. D. Andrade, and V. Hlady, *Adv. Polymer Sci,* 1986,79,1-63.

38 M. Rabe, D. Verdes, and S. Seeger, *Adv. Colloid Interface Sci,* 2011,162,87–106.

39 W. Lee, J. Jung, Y. K. Hahn, S. K. Kim, Y. Lee, J. Lee, T. Lee, J. Park, H. Seo, J. N. Lee, J. H. Oh, Y. Choi and S. S. Lee, *Analyst*, 2013, 138, 2558-2566.

40 D. Purvis, O. Leonardova, D. Farmakovsky and V. Cherkasov, *Biosens. Bioelectron.*, 2003, 18, 1385-1390.

